The International Journal of Advanced Manufacturing Technology (2025) 137:2257–2266
https://doi.org/10.1007/s00170-025-15236-0

ORIGINAL ARTICLE

Avoiding the formation of pores during laser welding of copper hairpins by dynamic beam shaping

Eveline Nicole Reinheimer[1] · Michael Haas[1] · Felix Zaiß[1] · Markus Omlor[2] · Christoph Spurk[3] · Alexander Olowinsky[4] · Felix Beckmann[5] · Julian Moosmann[5] · Christian Hagenlocher[1] · Rudolf Weber[1] · Thomas Graf[1]

Received: 27 September 2024 / Accepted: 7 February 2025 / Published online: 27 February 2025

Abstract
Any pores formed during laser welding of copper hairpins affect the structural integrity and the mechanical/electrical functionality of the joint. We report on investigations using synchrotron X-ray imaging techniques to observe the formation of the pores in the processing zone while welding. It was found that all pores are formed at the joint gap and that the small pores are distributed throughout the complete joint volume as a result of the melt flow induced by the movement of the laser beam. This insight has led to the development of a welding strategy that minimizes pore formation by avoiding the movement of the laser beam across the joint gap. This was achieved by rapid beam shaping based on coherent beam combining (CBC) technology.

Keywords Laser beam welding · Copper welding · Pore formation · Coherent beam combination

1 Introduction

The advantages of laser welding, such as precise control, high welding speeds, and minimal heat-affected zones, make it an attractive option for the manufacturing of intricate components like copper hairpins used in electrical and electronic applications. However, despite its many benefits, the process of laser welding can sometimes give rise to the formation of pores within the weld joints which can significantly compromise the structural integrity and functionality of the welded hairpins. In the case of copper hairpins, the intrusion of gases from the surrounding environment leads to the formation of small pores and of larger pores [1]. The localized heating and rapid cooling associated with laser welding can create favorable conditions for the entrapment of gases, particularly oxygen and nitrogen, which can diffuse into the weld pool from the surrounding atmosphere or from surface contaminants [2]. The formation of pores not only weakens the joint but also hinders the flow of electrical current, which is detrimental to the performance of the hairpins in electrical and electronic systems [3]. The occurrence and formation of pores in copper welding are still not fully understood and are subject of ongoing research as recently published work shows. Heider et al. [4] were able to show that the reason for pore formation in copper welding can be divided into process pores and gas pores. They concluded that process pores are caused by the instability of the capillary and gas pores are caused due to the interaction of the surrounding air and the melt pool, which can be influenced by the laser wavelength and the composition of the surrounding air. Kaufmann et al. [5] used in situ synchrotron x-ray imaging to investigate how the capillary is influenced by the process parameters. Other reports show that beam shaping [6, 7] or reducing the ambient pressure [8] is a useful method to reduce pores when welding copper. Laser welding of hairpins differs from other welding processes like butt welding or flange joints where the laser beam is usually moved in one pass along the joining gap. When welding hairpins, the laser beam is typically moved over the same contour many times

✉ Eveline Nicole Reinheimer
Eveline-nicole.reinheimer@ifsw.uni-stuttgart.de

1 IFSW, University of Stuttgart, Pfaffenwaldring 43, 70569 Stuttgart, Germany

2 Dr. Ing. h. c. F. Porsche AG, Porscheplatz 1, 70435 Stuttgart, Germany

3 Lehrstuhl Für Lasertechnik, RWTH Aachen, Steinbachstr. 15, 52074 Aachen, Germany

4 Fraunhofer-Institut Für Lasertechnik ILT, Steinbachstr. 15, 52074 Aachen, Germany

5 Helmholtz Zentrum Hereon, Notkestraße 85, 22607 Hamburg, Germany

until the desired joint cross-section is obtained. The vapor capillary and the melt pool grow deeper during the ongoing process. This is why the formation of pores can have other reasons as when conventionally welding butt, lap, or flange joints. The present work therefore investigates the formation of pores during hairpin welding. The benchmarking work presented in [9] reports on the influence that various beam shapes and different laser wavelengths have on the hairpin welding process and the resulting weld quality. A workflow to optimize the hairpin welding process based on a study using synchrotron radiation for diagnostics is proposed in [10]. The issue of pore formation in laser welding of copper hairpins has already been addressed by extensive research and development efforts. Various strategies, such as the use of shielding atmospheres [11], surface cleaning [12], and modifications of the welding parameters [10–16], have been explored to minimize or eliminate the formation of pores. The impact of surface treatment to remove the protective lacquer from the copper hairpins before welding on the occurrence of pores in the welded hairpins is discussed in [17]. The influence of a gap between the two hairpins on the joint cross-section of the welded pins and the pore volume has already been investigated in detail by [11], which led to the conclusion that a gap of up to 0.5 mm does not influence the weld result significantly. It was also reported in [18] that large process pores with a radius of $r_P \geq 0.1$mm occur at the joining gap between the two hairpins, whereas the smaller pores with $r_P < 0.1$mm are found in the whole joint volume after welding. The present work therefore focuses on the investigation of the formation of pores as caused by the movement of the laser beam across the joint between the hairpins. This present work was stimulated by the conjecture that the small pores are also created when the laser beam moves across the gap and are afterward distributed in the volume by the melt flow. High-speed video observation of the processing zone using high-brilliance synchrotron x-ray radiation has confirmed this point. The results show that the moving laser beam induces melt flows that distribute the small pores throughout the volume of the joint. This finding led to the development of a welding strategy in which coherent beam combining is used for rapid shaping of the otherwise stationary laser beam to create the weld, thereby minimizing the formation of pores.

2 Methods

The experiments were carried out at the Petra III facility of the German Electron Synchrotron DESY (Deutsches Elektronen Synchrotron) in Hamburg, which provides a high x-ray imaging resolution. The high-speed camera recording the x-ray images worked at a rate of 8000 frames per second. The full experimental setup is described in [19]. Cu-ETP hairpins were welded with an IPG YLS-6000-U laser with a maximum output power of 6 kW at a wavelength of 1.07 µm.

The first experiments were carried out to identify the mechanism leading to the generation of pores in conventional welding with a moving beam. Using a beam-delivery fiber with a core diameter of 100 µm to transport the laser beam to a Newson scanning system, together with a collimation and focusing lens with a focal length of 70 mm and 163 mm, respectively, resulted in a beam waist with a top-hat intensity distribution and a diameter of $d_f = 232\mu$m. The beam waist was positioned on the surface of the hairpins for all welds. The scanning system was used to move the beam on a circular path. The experiments were performed with weld speeds ranging between $v = 400\text{mm} \cdot \text{s}^{-1}$ and $v = 700\text{mm} \cdot \text{s}^{-1}$. Two different diameters, $d_{c,1} = 1.0$mm and $d_{c,2} = 1.6$mm, of the circular welding paths were used. The beam was moved along this circular path until all corners of the pins were molten. The number of passes required depends on the other parameters, as listed in Table 1.

The parameters were adapted in such a way that approximately the same volume was melted for all welded pairs of hairpins. A typical x-ray image recorded with a high-speed (HS) camera during the welding process is shown in Fig. 1. A varying thickness of the transirradiated material and varying attenuation coefficients (as a function of the physical state of the material) result in a locally varying attenuation of the transmitted x-ray beam. As a consequence of this varying attenuation and additional diffraction effects, it is possible to distinguish between the capillary, the solid material, the melted material, and the pores in the weld pool in the recorded images [20]. The contour of the liquidus-solidus line is illustrated by the dashed-dotted line in Fig. 1, as it is challenging to identify in the raw data with the naked eye.

To improve the image quality, a flat field correction was first applied which is described in detail in [21, 22], and the gradation curve of the contrast correction in the Adobe Photoshop software was then adjusted to improve the contrast between the solid and the liquid material seen in the pictures. This correction of the contrast allows to identify the contour

Table 1 Experimental parameters

Beam path	Laser power P	Welding speed v	Number of passes
$d_{c,1} = 1.0$mm	5.8 kW	400 mm · s^{-1}	7
		500 mm · s^{-1}	9
		600 mm · s^{-1}	11
		700 mm · s^{-1}	14
$d_{c,2} = 1.6$mm	5.8 kW	400 mm · s^{-1}	4
		500 mm · s^{-1}	6
		600 mm · s^{-1}	8
		700 mm · s^{-1}	9

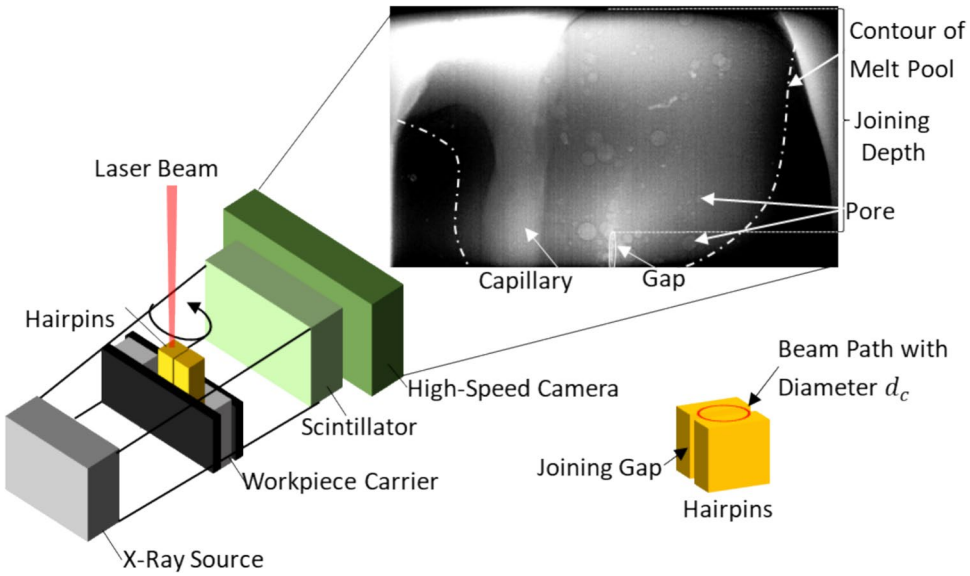

Fig. 1 Experimental set-up used to record the x-ray images of the welding process

of the liquidus-solidus line with the naked eye (Fig. 2). The scale in the x-ray images was determined by comparing the number of pixels showing the width of the copper hairpins with their actual width. Figure 2 compares a raw image during (a) and after the welding process (c) to the corresponding processed image (b, d), where the solidus–liquidus line is indicated by the blue arrows. In all the images shown in the following, the marked contour of the melt pool was identified using the processed images and subsequently overlaid onto the raw images, where the capillary and the pores are well visible. The analyzed videos are made available as supplementary material at [23].

CT analysis was used to determine the total volume V_m of the melt and the volume V_p of all the pores in the welded pins. A detailed description of this procedure is given in [18]. The liquidus-solidus contour determined in the x-ray images and the cross-sections of the produced joints was compared to the ones extracted from CT scans of the welded

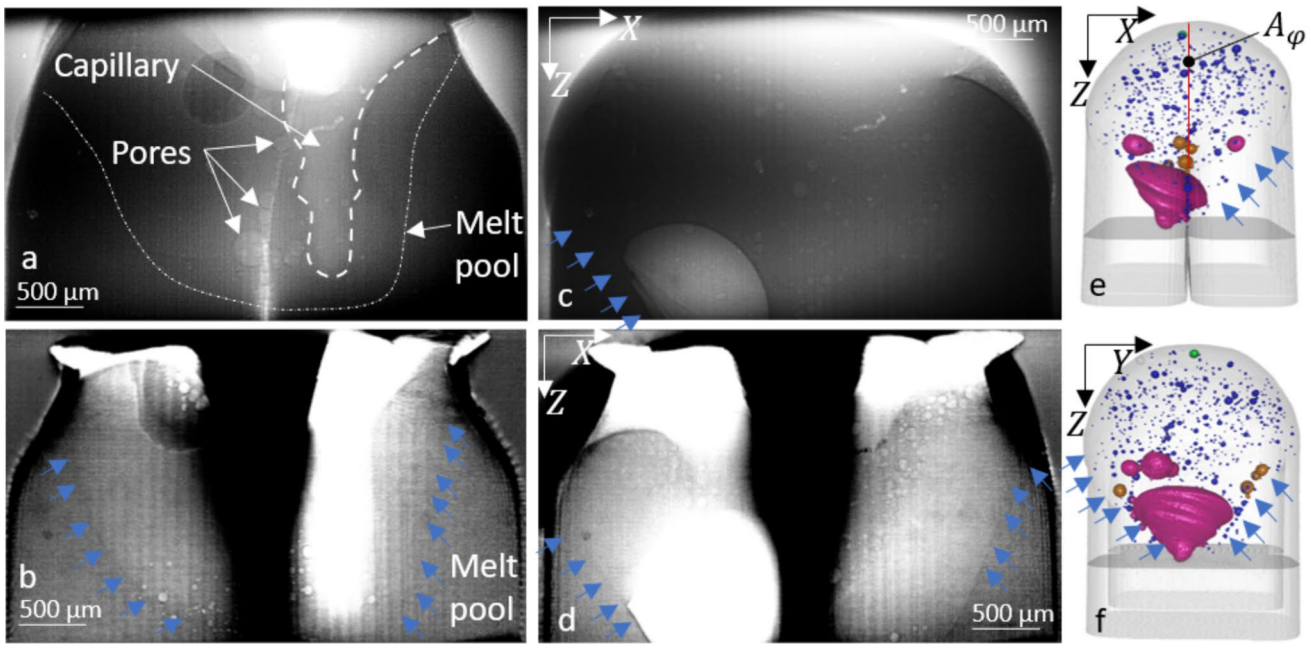

Fig. 2 Raw images recorded with the x-ray imaging system during the welding process (**a**) and after the welding process (**c**) to determine the contour of the capillary and the contours of pores and the corresponding processed image (**b, d**) to determine the contour of the melt pool which were compared to the CT scan (**e, f**)

hairpins, as shown in Fig. 2e and f to verify the scale of the x-ray images and CT scans. The ratio A_φ of the joint cross-section between the two pins (minus the area of the pores in this plane) to the cross-sectional area of a single pin is an important value for the design of electrical machines and should be > 1.

3 Results

The analysis of the high-speed x-ray videos revealed that the two different diameters of the welding path resulted in a significant difference in the shape and dimensions of the capillary and the melt pool formed during the welding process. Applying the small welding circles with $d_{c,1} = 1.0$mm, the capillary was found to be narrow and deep almost immediately after the beginning of the welding process, while, with the larger welding circles ($d_{c,2} = 1.6$mm), the capillary was wider and shallower and its depth increased only gradually with each pass, see Fig. 3.

In the weld with the smaller circle ($d_{c,1}$), the outline of the capillary is narrow and deep at a time $t = 34.5$ms after turning on the laser. The capillary reaches a depth of 2 mm and keeps approximately this depth throughout the whole welding process. At $t = 58.5$ms, the laser was switched off as the targeted volume of the melt pool was reached. Many small pores can be seen next to the joining gap between the two pins at the beginning of the weld at $t = 34.5$ms. At $t = 47.75$ms, the melt pool expands further outwards and many more pores are visible near the joining gap. A large pore remains at the bottom of the weld after the collapse of the capillary. After the complete solidification at $t = 162.5$ms, the pores are distributed over the entire area of the joint.

In the weld with the large circular path, the depth of the capillary increases from 1 mm at $t = 34.5$ms to 1.6 mm at $t = 47.75$ms (when the weld pool has a depth of 1.7 mm) and to 1.8 mm at $t = 52.75$ms (depth of weld pool is 1.9 mm). Simultaneously, the initially few and small pores visible along the joining gap ($t = 34.5$ms) increase in number ($t = 47.75$ms). At $t = 52.75$ms, a large proportion of the pores are still concentrated along the joint gap, but some small pores are now seen at other locations in the melt pool. Additional pores continue to be formed at the joining gap for the remainder of the process time. After the laser is switched off and the capillary collapses, a large pore is left, which can be seen in the lower left of the fully solidified pin in the picture taken at $t = 145$ms. It can also be seen that the many small pores that are mainly concentrated near the joint gap during the process are eventually distributed throughout the entire volume of the joint after turning off the laser. Nevertheless, with the small circular path, the laser beam is constantly closer to the joining gap, and more pores are visible during and after welding than what is observed with the path with the larger diameter.

The influence of the welding path and the welding speed on the ratio $R_V = \frac{V_p}{V_m}$ of the total volume V_p of all pores with respect to the total weld volume V_m was determined by means of CT analysis. The results are shown in Fig. 4. It was consistently observed that the welds created using the smaller path diameter $d_{c,1}$ exhibited a higher relative pore content R_V than the ones produced using the larger diameter $d_{c,2}$. The observations of pore formation as it is described above were made for the whole range of welding speeds considered here. Additionally, the ratio A_φ is shown in Fig. 4 using the ordinate on the right.

The results of our study indicate that the diameter of the circular welding path has a significant impact on the formation of pores when laser welding hairpin structures. It was specifically observed that a higher number of pores is generated when the laser is moved more frequently over the joining gap between the two hairpins, as was the case using the small path diameter. The small pores that are formed next to the gap are probably derived from oxides, chemical impurities, and residual contamination on the surfaces of the pins. While the majority of pores originate near the gap, it is noteworthy that these pores are consistently found distributed throughout the entire weld volume at the end of the process. The supplementary videos [22] illustrate that the flow within the melt pool, induced by the movement of the laser beam and persisting for some time after the laser is turned off, disperses the pores throughout the entire joint volume until the solidification process is completed.

The findings lead to the conclusion that

- The location of the pores in the solidified pin does not provide any information about the origin of the pores and their root cause (chemical contamination, oxides, residual varnish).
- The pores are generated by the passage of the laser beam over the gap between the pins.
- Large pores are mainly formed in the lower area of the weld.

It was therefore postulated that pores can be avoided if the movement of the laser beam across the gap between the two pins is avoided. From these results, it can be derived that for a defect-free weld, a stable capillary, which is not moved over the gap between the hairpins, is necessary. Such a process can be designed with newly available lasers featuring fast beam shaping. This can be realized by dynamic beam shaping as shown in the following example of coherent beam combining, by which discrete transitions between different intensity distributions were performed instead of a continuous motion of the laser beam.

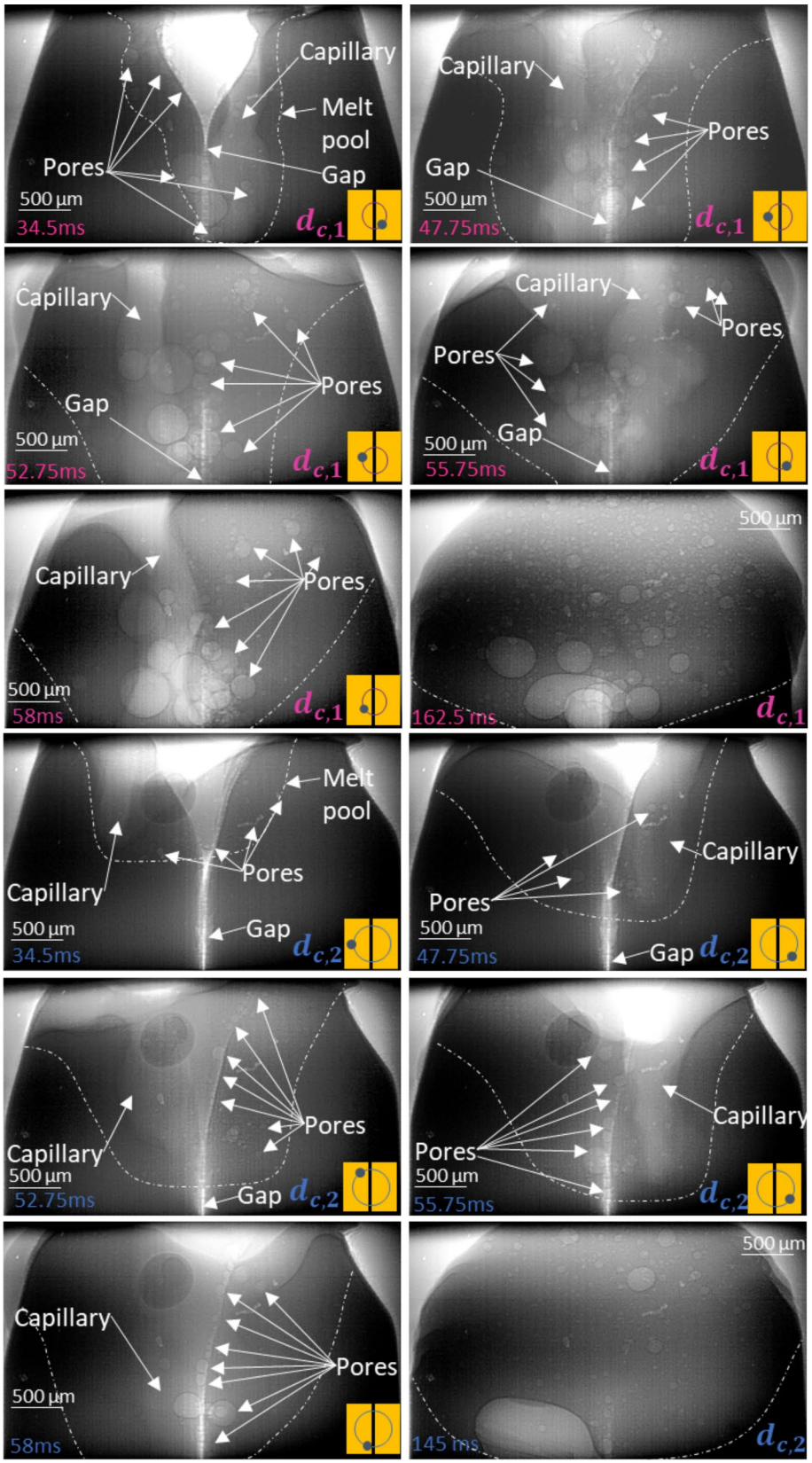

Fig. 3 X-ray images of the welding process at different instants of time t (indicated at the lower left corner of each image) after turning on the laser at $t=0$ for two different diameters of the circular welding paths: circular path with a diameter of 1 mm (purple) with 11 passes resulting in a process time of 58.5 ms and circular path with a diameter of 1.6 mm (blue) with 8 passes resulting in a process time of 67 ms. The position of the laser beam is indicated by the dots in the insets on the lower right corner of the images. For both welds, a laser power of 5.8 kW, a welding speed of 600 mms^{-1}, and a diameter of the beam waist of 232 mm were used. The scale shown at the top left applies to all the shown images

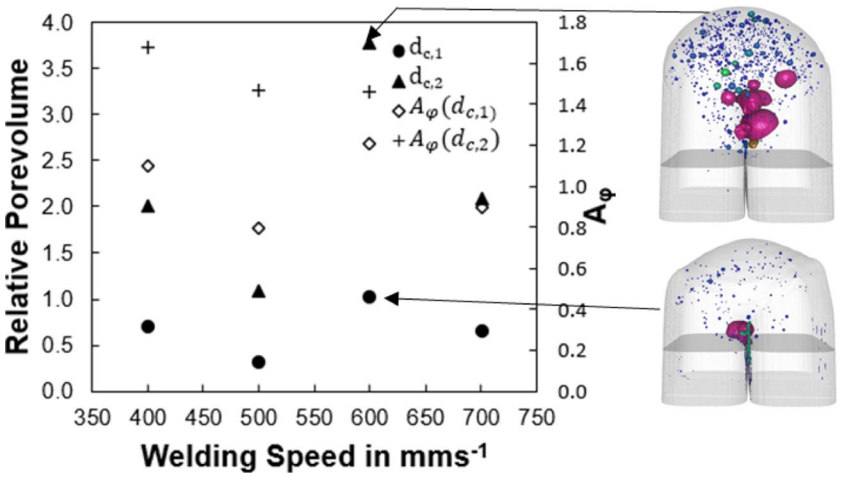

Fig. 4 Ratio R_V of the total pore volume with respect to the melted volume in the joint of the hairpins (left ordinate) welded with the path diameters $d_{c,1}$ (triangle) and $d_{c,2}$ (dots) at welding speeds ranging from $v = 400mm \cdot s^{-1}$ up to $v = 700mm \cdot s^{-1}$ and the determined ratio A_φ (right ordinate) for diameters $d_{c,1}$ (diamond) and $d_{c,2}$ (cross) as well as two CT scans of the welded pins at $v = 600mm \cdot s^{-1}$ where pores with $r_P < 0.1mm$ are indicated in blue and those with $r_P \geq 0.1mm$ are indicated in red and green

4 Process design

In order to implement a process strategy aimed at preventing pores, an approach was adopted where the laser beam remains stationary but rapidly changes its intensity distribution. This was achieved by employing the technology of coherent beam combination (CBC), as provided by the OPA6 laser from CIVAN, which is described in detail in [24, 25]. The setup used for our experiments is shown in Fig. 5. The x-ray imaging system used in following experiment to determine the shape of the keyhole by radiographing the processing zone in the transvers y-direction is described in detail in [21, 22, 26]. An x-ray tube FXE-224.48 by Yxlon with a minimum spot size of 6 µm and an acceleration voltage of 140 kV with a power of 85 W was used. A scintillator by Hamamatsu, Shizuoka, Japan, with 728×728 pixels with a resulting resolution of 58 pixel $\cdot$ mm^{-1} was used to convert the x-rays in visible light which was recorded with a high-speed camera SA3 from Photron. A typical x-ray image recorded by this system during the welding process is shown in Fig. 5. The welding process was video recorded from an inclined top-down perspective using a high-speed camera operating at a frame rate of 10 kHz, cf. Fig. 5.

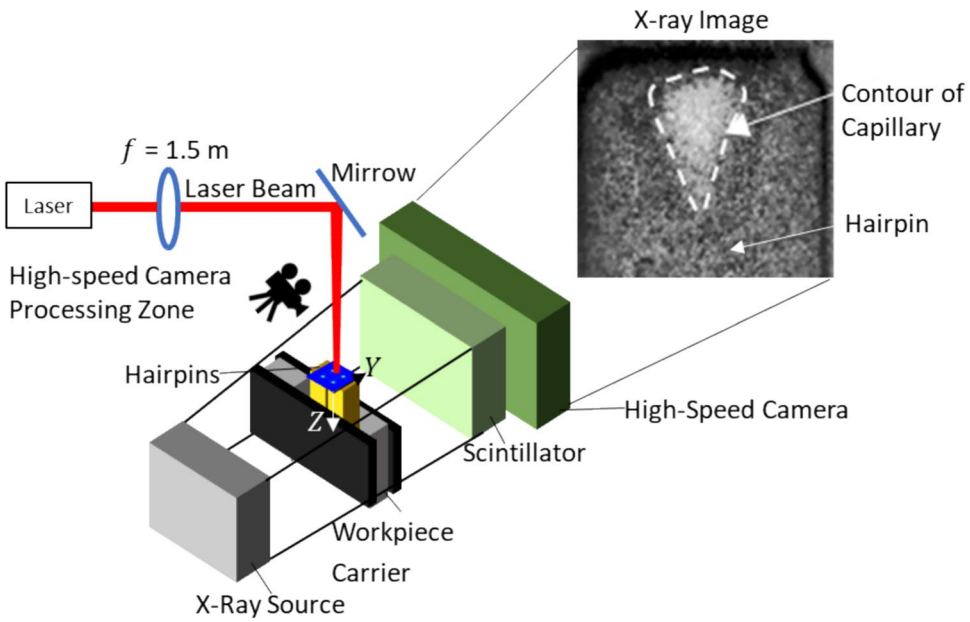

Fig. 5 Experimental set up with the OPA6 laser and the x-ray imaging system. An exemplary x-ray image of the processing zone is shown in the inset

Civan's OPA6 laser facilitates highly dynamic beam shaping by exploiting electro-optically controlled coherent beam combining 32 parallel fiber amplifiers in a phased array. A discussion of the principle and the technical implementation of coherent beam combining is beyond the scope of this paper which is why reference is made to [27, 28] for further details. Only the most important aspects and functions that are relevant to this work shall briefly be explained. Each laser beam of the 32 fiber lasers was focused at the same lateral position onto the surface of the hairpins by a lens with a focal length $f = 1\ 0.5\ m$. This results in a focal diameter of 900 μm for each beam. Coherent beam combining results in an interference that provides one local intensity maximum (main lobe) and additional interference peaks of higher orders (side lobes) within the illuminated area. The interference pattern can be repositioned with a high frequency by shifting the phase relationship of the individual laser beams.

The software of Civan provides 1024 possible positions of the main lobe, which exhibits a position-dependent peak intensity. The fast movement of the interference pattern which occurs at a frequency in the MHz range allows to create almost any arbitrary time-averaged intensity distributions [28]. Such a beam shape can be maintained for a preset duration t_{shape}, and the CBC technology allows to switch between different quasi-stationary intensity distributions within < 100 ns [27].

For the experiment, two different quasi-stationary time-averaged intensity distributions were generated, which both involve a total laser power of 9 kW. These two shapes and their position on the hairpins are sketched in Fig. 6. The system was programmed to switch periodically between these two beam shapes during the welding process. Each shape was present for a duration of $t_{\text{shape}} = 5\text{ms}$. Shape 1, the "four-spots shape" consists of the 4 local maxima shown on the left of Fig. 6 (color-coded). Shape 2, the "full-beam-field-shape" is composed of 256 positions of the interference pattern to form the wide time-averaged intensity distribution shown on the right in Fig. 6 (color-coded). The center of each of the two shapes was aligned at the center of the hairpins.

Figure 7 illustrates the state of the welding process at different instants of time t after the start of the laser welding process at $t = 0$. The first and fourth columns of Fig. 7 depict the beam shape at each time step and are shown in the orientation in which it is positioned on the hairpins shown next to it. The second and fifth columns show the images captured in the top-down view of the process. The third and sixth columns provide the corresponding x-ray images of the capillary. In column three, the contour of the hairpin is highlighted to guide the eye by the short-dashed line, and the contour of the vapor capillary is highlighted by the long-dashed line. The bottom row in columns five and six shows the welded hairpin from the top view and the corresponding x-ray image.

During the initial 10 ms of the process, the surfaces of each pin undergo separate melting, leading to the formation

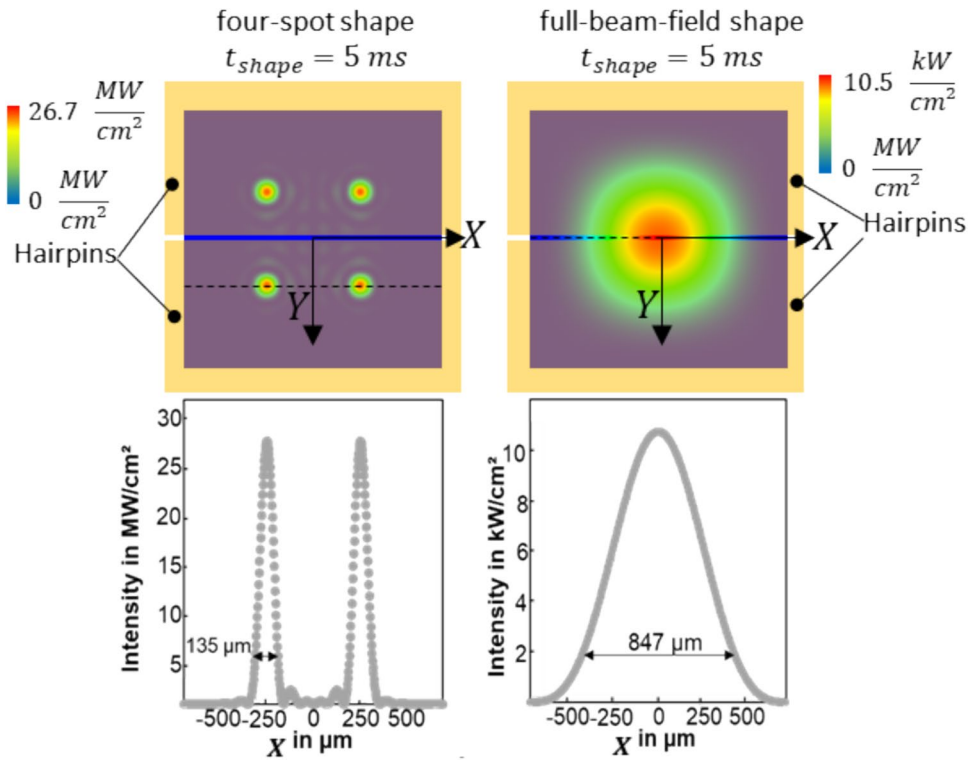

Fig. 6 The two alternatingly used (color-coded) intensity distributions of the laser beam and their position on the hairpins (top). The profiles of the intensity distribution along the dashed lines are shown in the lower part. The diameter of the constructive interference maxima is determined according to Din/En Iso 11146

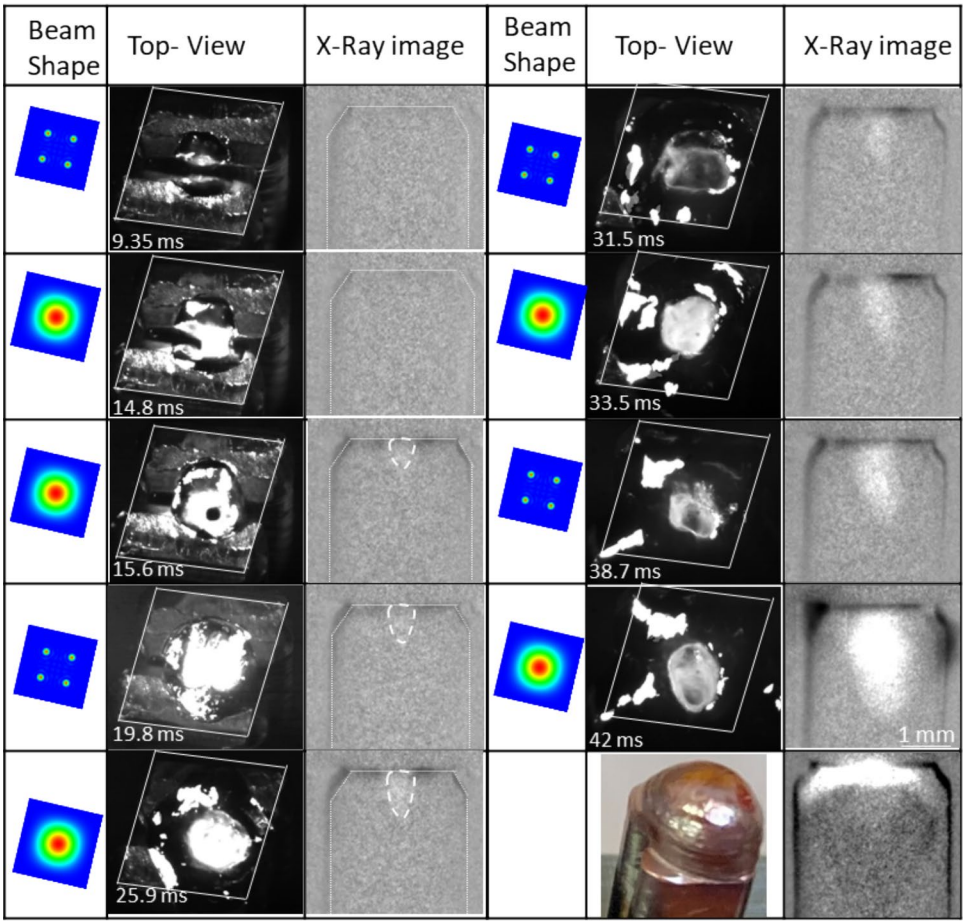

Fig. 7 X-ray images (third and sixth column) and corresponding images from the top-view (second and fifth column) of the welding process with the current beam shape (left column) at different instants of time (lower left corner) after turning on the laser at $t = 0$. The resulting cumulative image of the maximum gray values and a cross-section of the welded Pin are shown in the bottom line in the fifth and sixth columns. The whole process time was 42 ms, and a laser power of 9 kW was used

of two distinct melt pools as seen from the "top view" image on the upper left in Fig. 6. It can be seen from the "top-view" image just below that the two separate melt pools are merged at $t = 14.8$ms, creating a unified joint melt pool. Immediately after this, a capillary is formed at $t = 15.6$ms. The formation of a capillary is clearly visible in the corresponding x-ray image. In the ongoing process, the shape of the opening of the capillary on the surface undergoes alterations corresponding to the respective beam shapes. When the "four-dots shape" is present, an approximately square-shaped capillary is visible on the top, while a round capillary opening is visible when the "full-beam-field-shape" is present. The capillary is seen to progressively deepen with the advancing process time. Using these alternating beam shapes for welding, the capillary was found to remain stable while consistently increasing in depth and width. In the x-ray image of the welded hairpin (column six, bottom row), no large pores can be seen. Due to the noise in the x-ray image, no pores with a diameter $r_P < 0.1$mm can be determined in the images obtained from this setup; therefore, a cross-section was used to determine the presence of pores with $r_P < 0.1$mm. The cross-section of the welded hairpins is shown in Fig. 8.

The left picture in Fig. 8 shows that the process performed with the beam shaping approach described above results in a weld with minimal defects. Only a few small pores are visible in the cross-section. It can also be seen that the (resolidified) liquidus-solidus line is V-shaped. This differs from the course of this line seen in the cross-section of the joint welded with a movement of the laser beam (Fig. 8b). The V-shaped course of the liquidus-solidus line results in a thermally efficient joining process with a measured ratio $A_\varphi = 1.15$ that is sufficient for a good connection.

These findings confirm that employing a rapid sequence of different intensity distribution of a stationary beam rather than moving the beam on circles across the gap between the hairpins helps to stabilize the capillary and leads to a weld with only minor defects. Further research is needed to investigate the optimum intensity distribution and the influence of the frequency of the alternating beam shape on the stability of the capillary. In summary, both setups, the conventional laser process and the one performed with beam shaping by coherent beam combination, can be used to weld copper hairpins. With the proposed beam shaping, it is possible to weld the hairpins without moving the laser beam and therefore without moving the vapor capillary over the

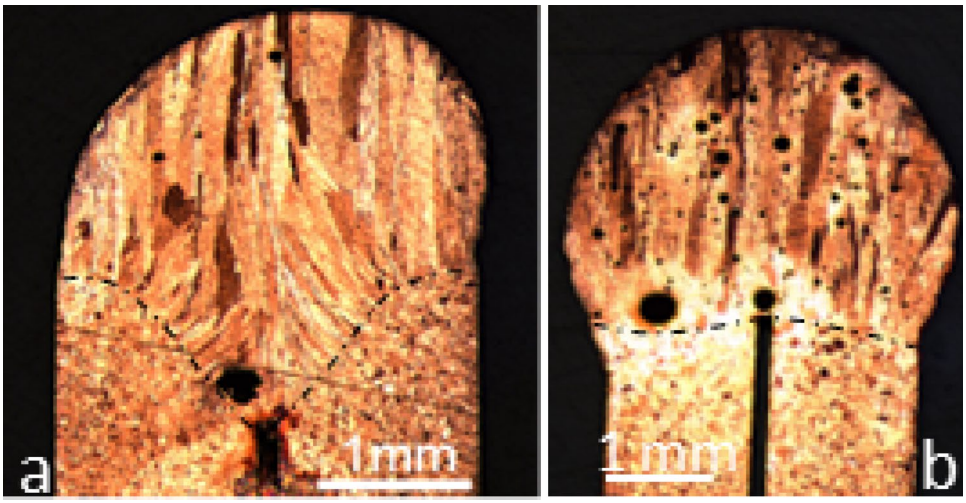

Fig. 8 Cross-section of the welded hairpin with coherent beam combination (**a**) and a cross-section of a hairpin welded with $d_{f_{c,1}}$ and a welding speed $v = 600\frac{\text{mm}}{\text{s}}$ and a laser power $P = 8\text{kW}$ (**b**) where the determined (resolidified) liquidus-solidus line is highlighted in the dotted-dashed line

gap. The results show that to avoid the formation of pores, it is beneficial not to move the capillary over the joint gap. Coherent beam combination is one possible solution to realize such a welding strategy.

5 Conclusion

In summary, we presented an investigation on the formation of pores that occur during welding of copper hairpins and proposed an approach to avoid this defect. The visualization based on synchrotron X-ray imaging techniques revealed that the pores are predominantly formed at the gap between the two pins each time when the beam crosses this position. The pores are then distributed throughout the entire weld volume due to melt flow induced by the movement of the laser beam. As a consequence, the location of the pores in the solidified pin does not provide any information about the origin of the pores and their root cause (chemical contamination, oxides, residual varnish). It has also been observed that large pores are mainly formed in the lower area of the weld.

Based on these findings, we proposed an approach that avoids the movement of the beam across the joint gap exploiting coherent beam combining to quickly change between two different quasi-stationary intensity distributions rather than moving the laser beam in circles. The results showed that this set-up allowed to significantly stabilize the vapor capillary which led to welding results with minimal defects.

Acknowledgements The research was partly funded in the framework of the industrial collective research program (IGF no. 22.058N). It was supported by the Federal Ministry for Economic Affairs and Energy (BMWi) through the AiF (German Federation of Industrial Research Associations eV) based on a decision taken by the German Bundestag. The presented investigations were partly carried out at RWTH Aachen University within the framework of the Collaborative Research Centre SFB1120-236616214 "Bauteilpräzision durch Beherrschung von Schmelze und Erstarrung in Produktionsprozessen" and partly funded by the Deutsche Forschungsgemeinschaft e.V. (DFG, German Research Foundation). The sponsorship and support are gratefully acknowledged. The experiments were carried out in cooperation with Helmholtz-Zentrum Hereon in Hamburg at DESY PETRA III, and we would like to thank all people involved for their support. The laser used for the experiments at Petra III (DESY, Hamburg) was provided by IPG Photonics Cooperation, and the laser used for the experiments with CBC was provided by Civan Advanced Technologies Ltd. The support of the funders and supporters is highly appreciated.

Funding Open Access funding enabled and organized by Projekt DEAL.

Declarations

Competing interests The authors declare no competing interests.

References

1. Alter L, Heider A, Bergmann JP (2020) Influence of hydrogen, oxygen, nitrogen, and water vapor on the formation of pores at welding of copper using laser light at 515 nm wavelength. J Laser Appl 32(2):22020
2. Kato E, Ueno H, Orimo T (1970) Solubility of hydrogen in liquid copper alloys. Trans JIM 11(5):351–358

3. Dimatteo V et al (2021) The effect of process parameters on the morphology, mechanical strength and electrical resistance of CW laser-welded pure copper hairpins. J Manuf Process 62:450–457
4. Heider A, Alter L (2024) Evaluation of pore formation during welding of copper using different laser sources. Procedia CIRP 124:383–387
5. Kaufmann F, Schrauder J, Hummel M, Spurk C, Olowinsky A, Beckmann F, Schmidt M (2024) Towards an understanding of the challenges in laser beam welding of copper–observation of the laser-matter interaction zone in laser beam welding of copper and steel using in situ synchrotron x-ray imaging. Lasers Manuf Mater Process 11(1):37–76
6. Spurk C, Dietrich F, Brüggenjürgen J, Hummel M, Häusler A, Olowinsky A, Moosmann J (2024) Analysis of laser beam welding with superimposed 445 and 1070 nm wavelength lasers on copper by in situ synchrotron diagnostics. J Laser Appl 36(4):042002
7. Kaufmann F, Roth S, Schmidt M (2024) Tailored laser beam shapes for welding of copper using green laser radiation. Int J Adv Manuf Technol, pp 1–20
8. Schleser M, Liebe P, Gerhards B, Gerhards B (2025) Laser beam welding of copper under vacuum to extend the process limits. Welding in the World, pp 1–12
9. D'Arcangelo S, Caprio L, Chesi D, Nocciolini D, Corbinelli R, Previtali B, Demir AG (2024) Comprehensive benchmarking of laser welding technologies including novel beam shapes and wavelengths for e-drive copper hairpins. Opt Laser Technol 169:109964
10. Hummel M, Spurk C, Heider A, Beranek M, Häusler A, Möller M, Moosmann J (2024) Development workflow based on in situ synchrotron investigations to optimize laser processing of copper pins. J Laser Appl 36(4):042001
11. Omlor M, Seitz N, Butzmann T, Petrich T, Gräf R, Hesse AC, Dilger K (2023) Quality characteristics and analysis of input parameters on laser beam welding of hairpin windings in electric drives. Weld World 67(6):1491–1508
12. Glaessel T, Seefried J, Franke J (2017) Challenges in the manufacturing of hairpin windings and application opportunities of infrared lasers for the contacting process. In: 2017 7th International Electric Drives Production Conference (EDPC). IEEE, pp 1–7
13. Bocksrocker O, Speker N, Beranek M, Hesse T (2019) Reduction of spatters and pores in laser welding of copper hairpins using two superimposed laser beams. In: Laser in Manufacturing Conference, Munich
14. Papastathopoulos E et al (2022) Advances in beam shaping of high-power CW lasers with BrightLine weld technology. In: High-Power Laser Materials Processing: Applications, Diagnostics, and Systems XI (vol 11994). SPIE, p 1199402
15. Lönn D, Spångberg D (2022) Study of process parameters in laser beam welding of copper hairpins
16. Tóth T, Hensel J, Thiemer S, Sieber P, Dilger K (2021) Electron beam welding of rectangular copper wires applied in electrical drives. Weld World 65:2077–2091
17. Sun T, Ademi S, Mishra S, Varsani D, McMahon R, Ceglarek D, Franciosa P (2024) Joining thin copper wire and copper busbar by remote laser welding for electric motor assembly: impact of welding parameters and pre-welding surface treatment. Sci Technol Weld Join 29(5–6):337–346
18. Omlor M, Reinheimer EN, Butzmann T, Dilger K (2023) Investigations on the formation of pores during laser beam welding of hairpin windings using a high-speed x-ray imaging system. J Laser Appl 35(3):032010
19. Wagner J, Hagenlocher C, Hummel M, Olowinsky A, Weber R, Graf T (2021) Synchrotron X-ray analysis of the influence of the magnesium content on the absorptance during full-penetration laser welding of aluminum. Metals 11(5):797
20. Kawahito Y, Wang H (2019) In-situ observation of laser manufacturing with X-ray technique. Synchrotron Radiat News 32(2):14–19
21. Abt F, Boley M, Weber R, Graf T (2011) X-ray videography for investigation of capillary and melt pool dynamics in different materials. In: ICALEO 2011: 30th International Congress on Laser Materials Processing, Laser Microprocessing and Nanomanufacturing. AIP Publishing, pp 179–186
22. Boley M, Fetzer F, Weber R, Graf T (2019) High-speed x-ray imaging system for the investigation of laser welding processes. J Laser Appl 31(4):042004
23. Supplementary Data: https://doi.org/10.18419/darus-4047
24. Shekel E, Vidne Y, Urbach B (2020) 16kW single mode CW laser with dynamic beam for material processing. In Fiber Lasers XVII: Technology and Systems Vol. 11260, pp 267–272
25. Prieto C, Vaamonde E, Diego-Vallejo D, Jimenez J, Urbach B, Vidne Y, Shekel E (2020) Dynamic laser beam shaping for laser aluminium welding in e-mobility applications. Procedia CIRP 94:596–600
26. Lind J, Hagenlocher C, Blazquez-Sanchez D, Hummel M, Olowinsky A, Weber R, Graf T (2021) Influence of the laser cutting front geometry on the striation formation analysed with high-speed synchrotron X-ray imaging. IOP Conf Ser: Mater Sci Eng 1135(1):012009
27. Shekel E (2024) Dynamic beam shaping with coherent beam combining: a description of the physics underlying coherent beam combining, capabilities and applications. PhotonicsViews 21(3):26–29
28. Weber R, Wagner J, Peter A, Hagenlocher C, Spira A, Urbach B, Vidne Y (2024) Basic properties of high-dynamic high-power coherent laser beam combining for materials processing